

Augmented Model Predictive Control: A Balance between Satellite Agility and Computation Complexity

Yiming Wang¹ and Mihindukulasooriya Sheral Crescent Tissera² and Haihong Yu²
and Kai Jie Ethan Foo² and Sean Yeo Keyuan² and Ankit Srivastava² and Hao An¹

Abstract—Agile earth observation satellites employ multiple actuators to enable flexible and responsive imaging capabilities. While significant advancements in actuator technology have enhanced satellites’ torque and momentum, relatively little attention has been given to control strategies specifically tailored to improve satellite agility. This paper provides a comparative analysis of different Model Predictive Control (MPC) formulations and introduces an augmented-MPC method that effectively balances agility requirements with hardware implementation constraints. The proposed method achieves the high-performance characteristics of nonlinear MPC while preserving the computational simplicity of linear MPC. Numerical simulations and physical experiments are conducted to validate the effectiveness and feasibility of the proposed approach.

I. INTRODUCTION

Earth Observation Satellites (EOSs) are spacecraft engineered to remotely monitor the Earth’s natural environment and human activities from orbit. Equipped with diverse sensors—including visible light cameras, multispectral imagers, and thermal infrared detectors—these satellites collect critical data about the Earth’s surface and the near-Earth atmosphere [1]. They serve as indispensable tools in various domains such as resource exploration, urban planning, environmental surveillance, and disaster assessment.

In recent years, small satellites weighing less than 50 kg and with dimensions smaller than a laser printer have gained widespread popularity. This trend is driven by advancements in commercial off-the-shelf technologies and the adoption of agile development approaches. These satellites have opened up space as the next frontier for civilization and are part of what the space industry has called “NewSpace”, which refers to the increased accessibility for commercialization in the private space sector and the recent exponential progress in the nano and micro satellite industry [2].

To broaden their observational capabilities, Agile EOSs (AEOSs) are outfitted with multiple actuators—such as reaction wheels and control moment gyroscopes—that enable full three-degree-of-freedom attitude control [3]. This agility allows AEOSs to perform off-nadir observations by adjusting their orientation, rather than relying solely on direct overhead passes [4]. As a result, AEOSs greatly improve the practicality of satellite scheduling problems, where observation tasks must be efficiently assigned within constrained time windows to maximize overall mission value [5].

Agility, in the context of satellite operations, refers to the ability to rapidly reorient in space. A satellite that can swiftly transition between tracking targets and maintain stable pointing performance is inherently more agile. Consequently, higher agility translates into enhanced reliability and flexibility in executing complex observation schedules.

Recent advancements have focused heavily on enhancing actuator performance—particularly by increasing the maximum torque and angular momentum output—which is fundamental to improving satellite agility. To enhance such agility, NewSpace companies have launched high-torque producing actuators such as miniaturized control moment gyroscopes. However, due to strict size, weight, and power constraints of small satellites, enhancing agility through hardware alone is not optimal. Thus, a critical yet frequently overlooked challenge is how to maximize the agility of satellites using low-power, cost-effective actuators. This leads to a key question: can advanced control strategies boost satellite agility without relying solely on hardware upgrades?

Model Predictive Control (MPC) has garnered significant attention in both academic and industrial communities for its ability to balance control precision and energy efficiency, particularly under actuator saturation constraints. Among its variants, Linear MPC (LMPC) is widely used in satellite systems due to its relatively low computational demands. For example, Zhao et al. highlighted the high computational requirements of MPC and proposed an advanced attitude controller based on LMPC [6]; similarly, Caverly et al. employed LMPC to retain low computational burden [7]. In contrast, Nonlinear MPC (NMPC) captures the system’s nonlinear dynamics more accurately and offers superior performance by optimizing a more realistic cost function [8]. Zhou et al. integrated an online model identification algorithm with NMPC and used Sequential Quadratic Programming (SQP) to solve the resulting Optimal Control Problem (OCP) [9]. Song et al. demonstrated that once an optimization objective is defined, NMPC with SQP can outperform reinforcement learning in control tasks [10]. Kamel et al. also reported that NMPC provides greater robustness and dynamic performance than LMPC in comparative experiments [11]. Nevertheless, these benefits come with a significantly higher computational cost, as the complexity of solving NMPC increases rapidly with the prediction horizon. This makes NMPC highly demanding in terms of onboard processing power [12], [13].

As reviewed in the literature, LMPC is generally preferred over NMPC for satellite attitude control due to its lower computational requirements. The high computational load

¹Department of Control Science and Engineering, Harbin Institute of Technology, Harbin, China 22b904002@stu.hit.edu.cn

²Department of Electrical and Computer Engineering, National University of Singapore, Singapore tsheral@nus.edu.sg

imposed by NMPC is particularly problematic for small satellites, leading to increased system complexity and cost. Moreover, NMPC often fails to achieve real-time performance because of its iterative optimization process, which can introduce unacceptable delays in time-sensitive aerospace missions. On the other hand, LMPC relies on simplified models, resulting in suboptimal solutions compared to NMPC and thus offering reduced agility. This presents a compelling challenge: how can one retain the superior performance of NMPC while preserving the computational efficiency of LMPC? To the best of the author's knowledge, no effective solution has been proposed. This paper addresses this gap by introducing an augmented-LMPC approach. By embedding an integrator into the baseline LMPC structure, the proposed method improves tracking agility without necessitating changes to the actuator hardware.

The remainder of this paper is structured as follows: Chapter II presents the satellite's kinematic and dynamic models, along with the baseline LMPC framework. Chapter III introduces the proposed augmented-LMPC method and formulates several OCPs for different MPC methods. Chapter IV provides comprehensive comparative experiments to evaluate the performance of different MPC methods. Finally, Chapter V concludes the paper with a summary of findings and potential future directions.

II. PRELIMINARIES

In this section, the nonlinear kinematic and dynamic models of the satellite are formulated. Based on these complete models, system linearization is performed.

A. Nonlinear Model

To avoid the singularity inherent in Euler angles, this paper employs quaternions to represent the satellite's attitude. The Earth-Centered Inertial (ECI) frame is selected as the inertial reference frame. Based on the satellite's orbital position, the quaternion representing the rotation from the ECI frame to the Local-Vertical/Local-Horizontal (LVLH) frame is first determined. This quaternion is then further rotated to align with the target frame, according to the target's relative latitude and longitude, yielding the target quaternion $\mathbf{q}_t \in \mathbb{R}^4$.

The attitude kinematics and dynamics of the satellite are given as follows [14]:

$$\dot{\mathbf{q}} = \frac{1}{2} \begin{bmatrix} q_0 & -q_1 & -q_2 & -q_3 \\ q_1 & q_0 & -q_3 & q_2 \\ q_2 & q_3 & q_0 & -q_1 \\ q_3 & -q_2 & q_1 & q_0 \end{bmatrix} \begin{bmatrix} 0 \\ \boldsymbol{\omega} \end{bmatrix} \quad (1)$$

$$\dot{\boldsymbol{\omega}} = \mathbf{J}^{-1} (\mathbf{T} - \boldsymbol{\omega} \times (\mathbf{J}\boldsymbol{\omega} + \mathbf{h}_{rw})) \quad (2)$$

where $\mathbf{q} = [q_0, q_1, q_2, q_3]^T$ denotes the satellite's attitude quaternion, $\boldsymbol{\omega} = [P, Q, R]^T$ is the angular rate, $\mathbf{T} \in \mathbb{R}^3$ represents the control torque generated by the reaction wheel, and $\mathbf{h}_{rw} \in \mathbb{R}^3$ is the reaction wheel momentum, which satisfies

$$\dot{\mathbf{h}}_{rw} = -\mathbf{T} \quad (3)$$

TABLE I: Satellite Moment of Inertia

Parameter	Value	Unit
J_{xx}	0.2912908	$\text{kg} \cdot \text{m}^2$
J_{yy}	0.2837495	$\text{kg} \cdot \text{m}^2$
J_{zz}	0.3940411	$\text{kg} \cdot \text{m}^2$
J_{xy}	-0.0024154	$\text{kg} \cdot \text{m}^2$
J_{xz}	0.0011626	$\text{kg} \cdot \text{m}^2$
J_{yz}	0.0009412	$\text{kg} \cdot \text{m}^2$

Here, $\mathbf{J} \in \mathbb{R}^{3 \times 3}$ is the satellite's inertia matrix, with the value listed in Table I.

The quaternion error $\mathbf{q}_e \in \mathbb{R}^4$ is defined as

$$\mathbf{q}_e = \mathbf{q} \otimes \mathbf{q}_t^{-1} \quad (4)$$

where the operator " \otimes " denotes quaternion multiplication.

B. Linearization

The error quaternion \mathbf{q}_e can be separated into two components, and the kinematic equation (1) is rewritten as

$$\dot{\mathbf{q}}_e = \begin{bmatrix} \dot{\eta} \\ \dot{\boldsymbol{\xi}} \end{bmatrix} = \frac{1}{2} \begin{bmatrix} -\boldsymbol{\xi}^T \\ \eta \mathbf{I}_{3 \times 3} + [\boldsymbol{\xi} \times] \end{bmatrix} \boldsymbol{\omega} \quad (5)$$

where η denotes the scalar part, $\boldsymbol{\xi} = [\xi_1, \xi_2, \xi_3]^T$ is the vector part, $\mathbf{I}_{3 \times 3}$ is the three-dimensional identity matrix, and $[\boldsymbol{\xi} \times] \in \mathbb{R}^{3 \times 3}$ is the skew-symmetric matrix corresponding to the cross-product operation:

$$[\boldsymbol{\xi} \times] = \begin{bmatrix} 0 & -\xi_3 & \xi_2 \\ \xi_3 & 0 & -\xi_1 \\ -\xi_2 & \xi_1 & 0 \end{bmatrix} \quad (6)$$

Applying a Taylor expansion around the equilibrium point $\boldsymbol{\xi} = \mathbf{0}$ and neglecting higher-order terms yields the linearized form [15]:

$$\dot{\boldsymbol{\xi}} = \frac{1}{2} \mathbf{I}_{3 \times 3} \boldsymbol{\omega} \quad (7)$$

Next, the dynamic equation (2) is reformulated as

$$\dot{\boldsymbol{\omega}} = \mathbf{J}^{-1} \mathbf{T}_c \quad (8)$$

where $\mathbf{T}_c \in \mathbb{R}^3$ denotes the feedforward control torque. The reaction wheel torque command is then expressed as

$$\mathbf{T} = \mathbf{T}_c + \boldsymbol{\omega} \times (\mathbf{J}\boldsymbol{\omega} + \mathbf{h}_{rw}) \quad (9)$$

Combining the linearized kinematic and dynamic models (7-8), the satellite attitude error dynamics in state-space form can be written as

$$\begin{cases} \dot{\mathbf{x}} = \mathbf{A}_1 \mathbf{x} + \mathbf{B}_1 \mathbf{T}_c \\ \mathbf{y} = \mathbf{C}_1 \mathbf{x} \end{cases} \quad (10)$$

where $\mathbf{x} = [\boldsymbol{\xi}; \boldsymbol{\omega}]$, $\mathbf{y} = \boldsymbol{\xi}$, and the system matrices are given by

$$\mathbf{A}_1 = \begin{bmatrix} \mathbf{0}_{3 \times 3} & \frac{1}{2} \mathbf{I}_{3 \times 3} \\ \mathbf{0}_{3 \times 3} & \mathbf{0}_{3 \times 3} \end{bmatrix}, \quad \mathbf{B}_1 = \begin{bmatrix} \mathbf{0}_{3 \times 3} \\ \mathbf{J}^{-1} \end{bmatrix}, \quad (11)$$

$$\mathbf{C}_1 = [\mathbf{I}_{3 \times 3}, \mathbf{0}_{3 \times 3}]$$

For a sampling time t_s , the discrete-time state-space model corresponding to (10) can be expressed as

$$\begin{cases} \mathbf{x}(k+1) = \mathbf{A}_2 \mathbf{x}(k) + \mathbf{B}_2 \mathbf{T}_c(k) \\ \mathbf{y}(k) = \mathbf{C}_2 \mathbf{x}(k) \end{cases} \quad (12)$$

with matrices defined as

$$\mathbf{A}_2 = e^{\mathbf{A}_1 t_s}, \quad \mathbf{B}_2 = \left(\int_0^{t_s} e^{\mathbf{A}_1 t} dt \right) \mathbf{B}_1, \quad \mathbf{C}_2 = \mathbf{C}_1 \quad (13)$$

III. METHODOLOGY

To systematically introduce different MPC strategies for satellite attitude control, we begin with the augmented model and then present several MPC formulations.

A. Augmented Model

Based on the discrete-time state-space equations (12), the augmented model is formulated as

$$\begin{cases} \mathbf{x}_a(k+1) = \mathbf{A}_a \mathbf{x}_a(k) + \mathbf{B}_a \Delta \mathbf{T}_c(k) \\ \mathbf{y}_a(k) = \mathbf{C}_a \mathbf{x}_a(k) \end{cases} \quad (14)$$

where $\mathbf{x}_a(k) = [\Delta \mathbf{x}(k); \mathbf{y}_a(k)]$ and $\mathbf{y}_a(k) = \mathbf{y}(k)$. The operator Δ denotes a difference, with $\Delta \mathbf{x}(k) = \mathbf{x}(k) - \mathbf{x}(k-1)$ and $\Delta \mathbf{T}_c(k) = \mathbf{T}_c(k) - \mathbf{T}_c(k-1)$ representing the increment of state variables and control torques, respectively. The corresponding matrices are expressed as

$$\mathbf{A}_a = \begin{bmatrix} \mathbf{A}_2 & \mathbf{0}_{3 \times 3} \\ \mathbf{C}_2 \mathbf{A}_2 & \mathbf{I}_{3 \times 3} \end{bmatrix}, \quad \mathbf{B}_a = \begin{bmatrix} \mathbf{B}_2 \\ \mathbf{C}_2 \mathbf{B}_2 \end{bmatrix}, \quad (15)$$

$$\mathbf{C}_a = [\mathbf{0}_{3 \times 6}, \mathbf{I}_{3 \times 3}]$$

B. Augmented-Constrained LMPC (CLMPC)

From the augmented model (14), the predicted output over the horizon is obtained as

$$\mathbf{y}_a(k) = \Phi_a \mathbf{x}_a(k) + \mathbf{R}_a \Delta \mathcal{T}_c(k) \quad (16)$$

where $\mathbf{y}_a(k) = [\mathbf{y}_a(k+1); \mathbf{y}_a(k+2); \dots; \mathbf{y}_a(k+N_p)]$, with N_p denoting the prediction horizon. The control sequence is $\Delta \mathcal{T}_c(k) = [\Delta \mathbf{T}_c(k); \Delta \mathbf{T}_c(k+1); \dots; \Delta \mathbf{T}_c(k+N_c-1)]$, where N_c is the control horizon and $N_c \leq N_p$. The matrices are expanded as

$$\Phi_a = \begin{bmatrix} \mathbf{C}_a \mathbf{A}_a \\ \mathbf{C}_a \mathbf{A}_a^2 \\ \vdots \\ \mathbf{C}_a \mathbf{A}_a^{N_p} \end{bmatrix}, \quad (17)$$

$$\mathbf{R}_a = \begin{bmatrix} \mathbf{C}_a \mathbf{B}_a & \mathbf{0}_{3 \times 3} \\ \mathbf{C}_a \mathbf{A}_a \mathbf{B}_a & \mathbf{C}_a \mathbf{B}_a \\ \vdots & \vdots \\ \mathbf{C}_a \mathbf{A}_a^{N_p-1} \mathbf{B}_a & \mathbf{C}_a \mathbf{A}_a^{N_p-2} \mathbf{B}_a \\ \cdots & \mathbf{0}_{3 \times 3} \\ \cdots & \mathbf{0}_{3 \times 3} \\ \vdots & \vdots \\ \cdots & \mathbf{C}_a \mathbf{A}_a^{N_p-N_c} \mathbf{B}_a \end{bmatrix}$$

The associated cost function is defined as

$$J(k) = \mathcal{Y}_a^T(k) \mathcal{Y}_a(k) + W_{Augmented-CLMPC} \Delta \mathcal{T}_c^T(k) \Delta \mathcal{T}_c(k) \quad (18)$$

where $W_{Augmented-CLMPC}$ is a weight to balance tracking accuracy and control energy. Thus, the satellite attitude tracking problem can be formulated as the following OCP:

$$\begin{aligned} & \underset{\Delta \mathcal{T}_c(k)}{\operatorname{argmin}} \quad J(k) \\ & \text{s.t.} \quad \mathbf{T}_{min} \leq \mathbf{T}_c(k+i) \leq \mathbf{T}_{max}, \\ & \quad i = 0, 1, \dots, N_c - 1 \\ & \quad \mathbf{h}_{min} \leq \mathbf{h}_{rw} - t_s \sum_{j=0}^i \mathbf{T}_c(k+j) \leq \mathbf{h}_{max}, \\ & \quad i = 0, 1, \dots, N_c - 1 \end{aligned} \quad (19)$$

Here, \mathbf{T}_{min} and \mathbf{T}_{max} denote torque limits of the reaction wheel, while \mathbf{h}_{min} and \mathbf{h}_{max} represent the corresponding momentum bound. In this paper, the quadratic programming is solved using qpOASES [16]. Following the receding horizon strategy of MPC, only the first set of computed torque is applied at each step.

For further performance comparison, several alternative MPC formulations and their corresponding OCPs are summarized below.

C. Unconstrained LMPC (ULMPC)

In our previous work [15], [17], to minimize algorithmic complexity, torque and momentum constraints of the reaction wheel were omitted. From the discrete-time model (12), the predicted output is given by

$$\mathcal{Y}(k) = \Phi \mathbf{x}(k) + \mathbf{R} \mathcal{T}_c(k) \quad (20)$$

where $\mathcal{Y}(k) = [\mathbf{y}(k+1); \mathbf{y}(k+2); \dots; \mathbf{y}(k+N_p)]$ and $\mathcal{T}_c(k) = [\mathbf{T}_c(k); \mathbf{T}_c(k+1); \dots; \mathbf{T}_c(k+N_c-1)]$. The matrices are defined as

$$\Phi = \begin{bmatrix} \mathbf{C}_2 \mathbf{A}_2 \\ \mathbf{C}_2 \mathbf{A}_2^2 \\ \vdots \\ \mathbf{C}_2 \mathbf{A}_2^{N_p} \end{bmatrix}, \quad (21)$$

$$\mathbf{R} = \begin{bmatrix} \mathbf{C}_2 \mathbf{B}_2 & \mathbf{0}_{3 \times 3} \\ \mathbf{C}_2 \mathbf{A}_2 \mathbf{B}_2 & \mathbf{C}_2 \mathbf{B}_2 \\ \vdots & \vdots \\ \mathbf{C}_2 \mathbf{A}_2^{N_p-1} \mathbf{B}_2 & \mathbf{C}_2 \mathbf{A}_2^{N_p-2} \mathbf{B}_2 \\ \cdots & \mathbf{0}_{3 \times 3} \\ \cdots & \mathbf{0}_{3 \times 3} \\ \vdots & \vdots \\ \cdots & \mathbf{C}_2 \mathbf{A}_2^{N_p-N_c} \mathbf{B}_2 \end{bmatrix}$$

The corresponding OCP is

$$\underset{\mathcal{T}_c(k)}{\operatorname{argmin}} \quad \mathcal{Y}^T(k) \mathcal{Y}(k) + W_{ULMPC} \mathcal{T}_c^T(k) \mathcal{T}_c(k) \quad (22)$$

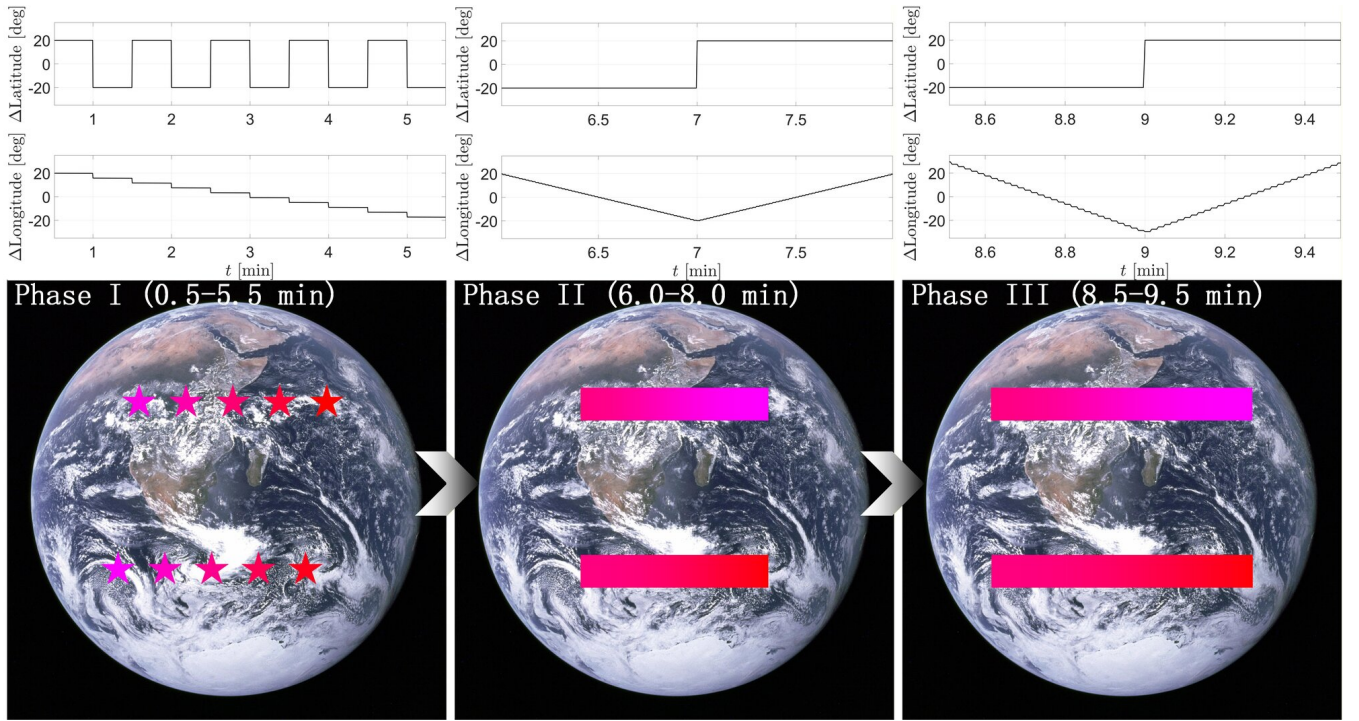


Fig. 1: Target latitude and longitude offsets in three phases.

D. CLMPC

Extending ULMPC, the CLMPC incorporates torque and momentum constraints. Its OCP is formulated as

$$\begin{aligned}
 \underset{\mathcal{T}_c(k)}{\operatorname{argmin}} \quad & \mathbf{Y}^T(k)\mathbf{Y}(k) + W_{CLMPC}\mathcal{T}_c^T(k)\mathcal{T}_c(k) \\
 \text{s.t.} \quad & \mathbf{T}_{min} \leq \mathbf{T}_c(k+i) \leq \mathbf{T}_{max}, \\
 & i = 0, 1, \dots, N_c - 1 \\
 & \mathbf{h}_{min} \leq \mathbf{h}_{rw} - t_s \sum_{j=0}^i \mathbf{T}_c(k+j) \leq \mathbf{h}_{max}, \\
 & i = 0, 1, \dots, N_c - 1
 \end{aligned} \tag{23}$$

E. NMPC

Unlike the LMPC formulation, the NMPC considers the full nonlinear model and is formulated as the following OCP:

$$\begin{aligned}
 \underset{\mathcal{T}}{\operatorname{argmin}} \quad & \sum_{k=0}^{N-1} \left(\bar{\mathbf{q}}_{e,k}^T \bar{\mathbf{q}}_{e,k} + W_{NMPC} \mathbf{T}_k^T \mathbf{T}_k \right) \\
 \text{s.t.} \quad & \bar{\mathbf{q}}_{e,k+1} = \mathbf{f}(\mathbf{q}_{e,k}, \boldsymbol{\omega}_k, \mathbf{T}_k) \\
 & \mathbf{T}_{min} \leq \mathbf{T}_k \leq \mathbf{T}_{max}, k = 0, 1, \dots, N-1 \\
 & \mathbf{h}_{min} \leq \mathbf{h}_{rw,k} \leq \mathbf{h}_{max}, k = 0, 1, \dots, N-1
 \end{aligned} \tag{24}$$

where $*_k$ denotes the variable at time kt_s , $\bar{\mathbf{q}}_e$ is the vector part of the quaternion error \mathbf{q}_e , $\mathcal{T} = \{\mathbf{T}_0, \mathbf{T}_1, \dots, \mathbf{T}_{N-1}\}$ is the control sequence, and $\mathbf{f}(\ast)$ represents the discretized form of Eqs (1-4). Here, N is the prediction horizon of NMPC. The nonlinear OCP is solved using SQP approach implemented via the ACADO toolkit [18], with qpOASES employed as the underlying quadratic programming solver [16].

IV. RESULTS AND DISCUSSION

A. Simulation Scenario

The simulations have been conducted using a dedicated simulator for attitude determination and control system developed by National University of Singapore (NUS) and can be found in [15]. Ten minutes of position and velocity data are obtained from the NUS satellite. Based on these data, together with the orbital parameters provided in [15], the time-varying rotation quaternion from the ECI frame to the LVLH frame, denoted as $\mathbf{q}_{LVLH/ECI}$, is generated. To compare the agility of different MPC methods, we define the rotation quaternion $\mathbf{q}_{\text{Target}/LVLH}$, which represents the transformation from the LVLH frame to the target frame. The target frame is determined by applying rotations to the LVLH frame according to the prescribed latitude and longitude offsets of the target point relative to the subsatellite point on the Earth's surface. The target quaternion can be obtained as

$$\mathbf{q}_t = \mathbf{q}_{\text{Target}/LVLH} \otimes \mathbf{q}_{LVLH/ECI} \tag{25}$$

To enable a comprehensive assessment of both agility and stability among different MPC methods, three phases in ten minutes are designed, as illustrated in Fig. 1.

- **Phase I (0.5–5.5 min):** The satellite sequentially points to ten different locations, issuing a reorientation command every 30 seconds. This scenario is used to simulate rapid imaging of multiple areas.
- **Phase II (6.0–8.0 min):** The satellite continuously tracks a target whose longitude drifts at a rate of 0.67 deg/sec. This scenario is used to simulate rapid ground scanning.

TABLE II: Simulation Environment

Parameter	Value	Unit
$noise_{gyro}$	0.27	deg/s
$noise_{rw}$	5	rpm
t_s	2	sec
T_{max}	4.18×10^{-3}	Nm
T_{min}	-4.18×10^{-3}	Nm
h_{max}	1.84×10^{-2}	Nms
h_{min}	-1.84×10^{-2}	Nms

TABLE III: Controller Parameters

Parameter	Value
N_p	10
N_c	10
N	10
$W_{Augmented-CLMPC}$	40
W_{ULMPC}	10
W_{CLMPC}	10
W_{NMPC}	10

- **Phase III (8.5–9.5 min):** The rate of change of the target’s longitude is further increased to 2 deg/sec. This scenario is used to investigate the agility limits of different MPC methods.
- **Others (0.0–0.5 min, 5.5–6.0 min, 8.0–8.5 min, 9.5–10.0 min):** The Target frame is aligned with the LVLH frame, i.e., $\Delta\text{Latitude} = \Delta\text{Longitude} = 0$.

The transition intervals between phases (denoted as “Others”) are included to allow the satellite to stabilize and to ensure consistent initial conditions for subsequent maneuvers. For practical considerations, appropriate levels of noise are added to both the gyroscope and the reaction wheel. The detailed simulation environment is summarized in Table II. To ensure a fair comparison, all MPC methods are implemented with the same prediction horizon, and the specific control parameters used in the simulations are listed in Table III.

B. Simulation Results and Discussion

Fig. 2 illustrates the attitude tracking error obtained from ten Monte Carlo simulations, while the corresponding quantitative results are summarized in Table IV. Throughout all phases, the ULMPC method, which does not account for actuator saturation, exhibits noticeable overshoots during rapid maneuvers and shows the longest transition time among all MPC methods. When actuator saturation is explicitly considered, CLMPC effectively limits excessive control effort. However, similar to ULMPC, it still exhibits steady-state errors in Phases II and III, when the target is in motion. The steady-state error arises from model mismatches in LMPC caused by system linearization and feedforward control, and its magnitude increases with the target’s motion speed. In contrast, the augmented-CLMPC employs an embedded integrator to compensate for model mismatches, thereby maintaining near-zero tracking errors

in all phases. Moreover, the augmented-CLMPC also shortens the transition time compared to other LMPC methods. Unlike LMPC-based methods, the NMPC captures the full nonlinear dynamics, achieving a faster transient response and maintaining near-zero steady-state error. Overall, ULMPC is limited by actuator constraints, while CLMPC enhances dynamic performance but still exhibits steady-state errors, whereas augmented-CLMPC and NMPC demonstrate superior accuracy and agility across all phases.

This paper considers a commercial camera with a swath angle of 0.8022 deg. The target is deemed observable when the satellite’s attitude tracking error remains within this angular range. Fig. 3 shows the observability percentages of different MPC methods over ten Monte Carlo simulations. The ULMPC exhibits longer transition time, which reduces the observable duration (with an average of 10.7 sec of full observability per area) during Phase I. Although CLMPC shortens the transition time (achieving an average of 12.9 sec of full observability per area), it still fails to maintain observability in Phases II and III due to steady-state errors when the target is in motion. In contrast, the augmented-CLMPC (achieving an average of 12.7 sec of full observability per area) maintains a high level of observability comparable to NMPC (achieving an average of 12.9 sec of full observability per area). Both methods achieve nearly continuous target observability across all phases, demonstrating their effectiveness in handling agile tracking tasks.

To further assess the reliability of different MPC methods in managing agile maneuvers, Fig. 4 presents the cumulative tracking error and actuator energy consumption during the transition and steady-state periods of Phase III. ULMPC and CLMPC accumulate more errors in both periods despite using similar amounts of energy (within the neighbourhood of $8 \times 10^{-4} \text{ N}^2 \cdot \text{m}^2$ during the transition period and $4 \times 10^{-5} \text{ N}^2 \cdot \text{m}^2$ during the steady-state period), reflecting their limited agility. The augmented-CLMPC accumulates 73.9% and 76.3% of the transition-period error of ULMPC and CLMPC, respectively, which is only 6.1% higher than that of NMPC. In the steady-state period, its cumulative error reduces to 5.5% and 5.4% of that of ULMPC and CLMPC, respectively, and matches the performance of NMPC.

In summary, the proposed augmented-CLMPC demonstrates agility comparable to NMPC while outperforming both ULMPC and CLMPC in both tracking precision and transition performance. Nevertheless, numerical simulations do not adequately reflect the computational burden of different MPC methods. Therefore, the following subsection presents experimental results to further evaluate the real-time feasibility of four controllers.

C. Experimental Results and Discussion

The experimental validation is conducted on a satellite attitude control platform mounted on an air-bearing table, which enables near-frictionless rotational motion, as shown in Fig. 5. A light source is used to emulate the Sun, and the satellite is equipped with sun sensors to continuously measure the incident direction of the light. The yaw reference

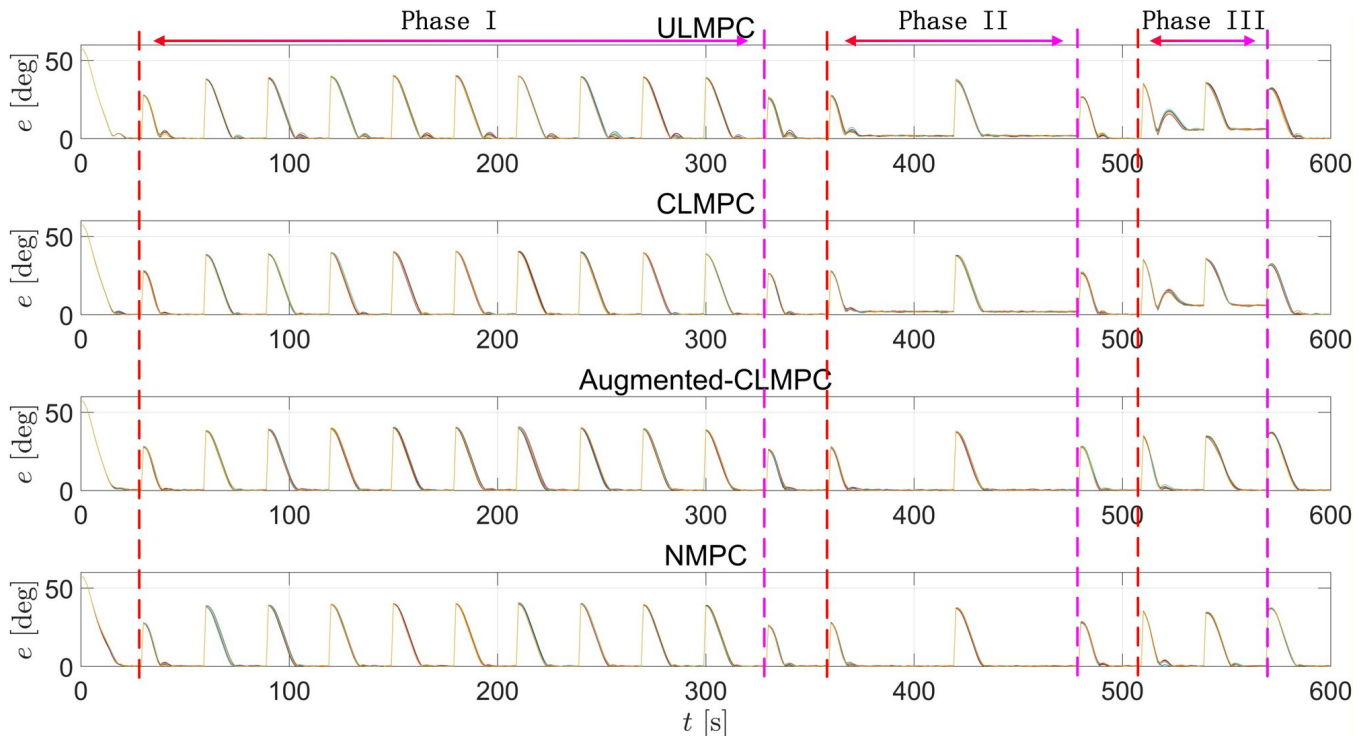


Fig. 2: Attitude error angle derived from quaternion error over ten Monte Carlo simulations.

TABLE IV: Quantitative results from ten Monte Carlo simulations.

Controller	ULMPC			CLMPC			Augmented-CLMPC			NMPC		
	Phase I	Phase II	Phase III	Phase I	Phase II	Phase III	Phase I	Phase II	Phase III	Phase I	Phase II	Phase III
TT ^a [s]	18.7	14.9	16.8	17.1	14.1	16.9	14.2	13.5	15.5	15.0	13.3	15.7
SSE ^b [deg]	0.23	1.99	6.04	0.26	1.97	5.97	0.34	0.37	0.37	0.33	0.35	0.34
MSE ^c [deg ²]	0.11	4.04	36.63	0.12	4.16	37.48	0.14	0.17	0.14	0.12	0.12	0.13

^aTT= Average transition time per area; ^bSSE= Average steady-state error; ^cMSE= Mean squared error in the steady-state period.

command is therefore generated according to the relative position of the light source, allowing the satellite to perform continuous yaw tracking. This setup enables a realistic comparison of different MPC methods in terms of their tracking performance and computational feasibility.

The NMPC solves OCPs by iteratively performing gradient descent of the cost function. As a result, considering the full nonlinear dynamics, NMPC requires substantially higher computational resources compared with LMPC, which relies on linearized and simplified models. Fig. 6 presents the average runtime of each MPC method per control update on the experimental platform. It can be observed that the augmented-CLMPC, similar to other LMPC methods, computes the optimal torque within approximately 0.3 sec, whereas NMPC requires about 2.2 sec—exceeding the control sampling period (2 sec). Such a high computational demand introduces intrinsic delay in generating the optimal torque, preventing NMPC from stably tracking the agile command in real-time experiments.

In the experiment, the yaw reference command oscillates between ± 32 deg at an angular rate of 1 deg/sec. The

tracking performance of different MPC methods is illustrated in Fig. 7. As observed, consistent with the numerical simulation results, the proposed augmented-CLMPC successfully eliminates the steady-state error. Quantitatively, its cumulative tracking error is reduced to 69.9% of that of ULMPC and 45.4% of that of CLMPC, while the reaction wheel energy consumption decreases to 77.9% and 51.7% of theirs, respectively.

V. CONCLUSION

This paper proposes an augmented-CLMPC algorithm that enables AEOs to achieve NMPC-level agility without incurring its substantial computational burden. Comprehensive numerical simulations and physical experiments demonstrate that the proposed controller not only eliminates the steady-state error inherent to conventional LMPCs but also achieves faster transient responses and reduced energy consumption. These results indicate that the augmented-CLMPC provides a practical balance between agility and computational complexity. The proposed method establishes an upper bound on the achievable agility of small satellites, which are often con-

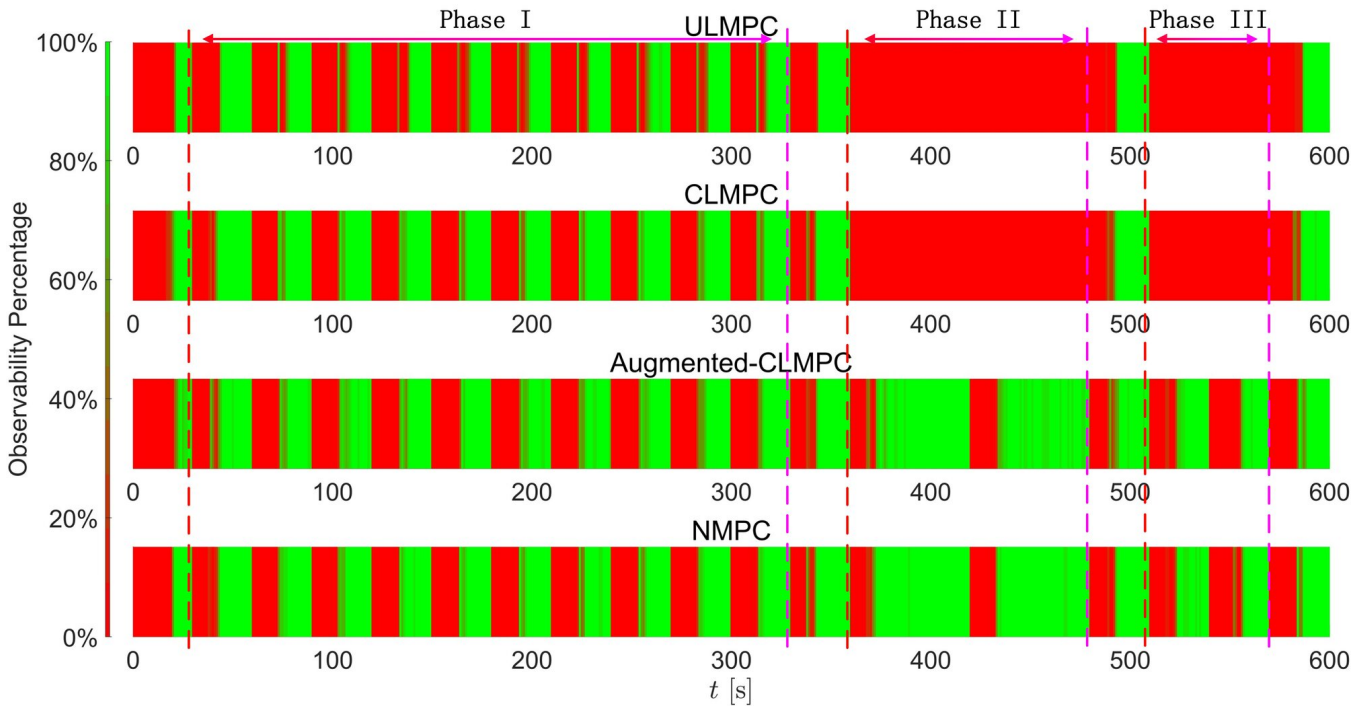
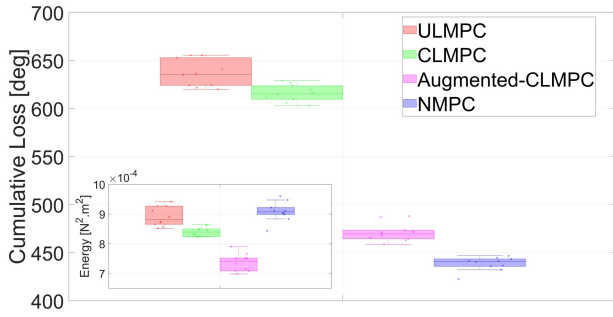
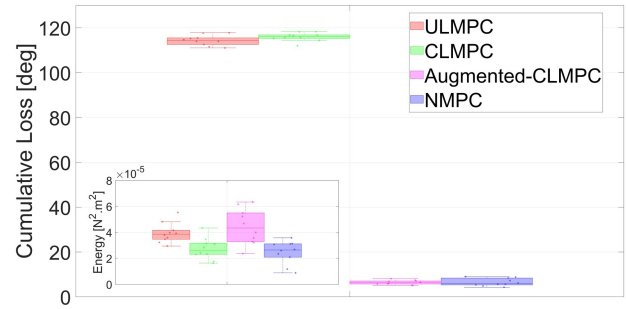


Fig. 3: Target observability percentage over ten Monte Carlo simulations.



(a) Transient period.



(b) Steady-state period.

Fig. 4: Cumulative loss and energy consumption during phase III.

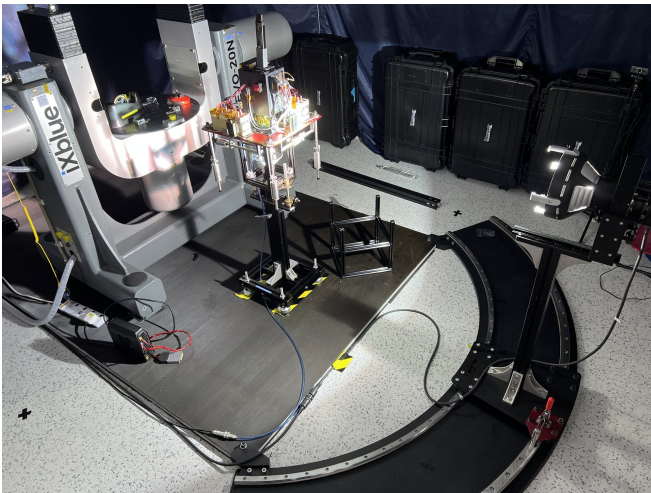


Fig. 5: Experimental platform for satellite attitude determination and control system [15], [19].

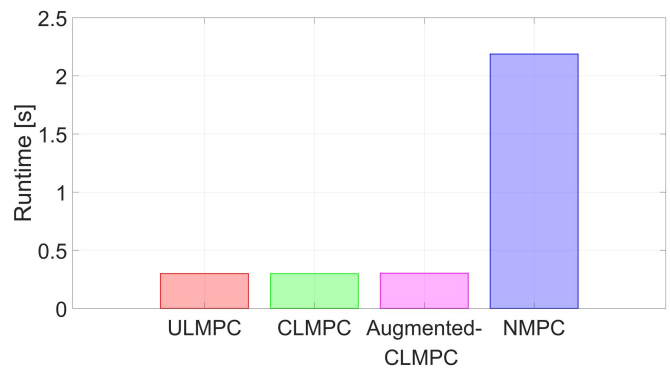


Fig. 6: Runtime required to deploy different MPC methods.

strained by limited size, weight, and power, and therefore lack the computational resources required by NMPC. It enables effective agile tracking even with limited actuation capability.

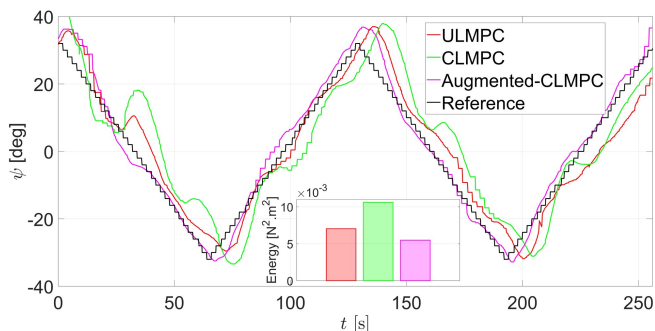


Fig. 7: Yaw tracking performance and energy consumption of different MPC methods.

Future work will focus on extending this framework to on-orbit applications and further exploring the agility potential of resource-constrained satellites [19], [20], [21].

REFERENCES

- [1] G. Soldi, D. Gaglione, N. Forti, A. D. Simone, F. C. Daffin'a, G. Bottini, D. Quattrociochi, L. M. Millefiori, P. Braca, S. Carniel, P. Willett, A. Iodice, D. Riccio, and A. Farina, "Space-based global maritime surveillance. part i: Satellite technologies," *IEEE Aerospace and Electronic Systems Magazine*, vol. 36, no. 9, pp. 8–28, 2021.
- [2] M. N. Sweeting, "Modern small satellites-changing the economics of space," *Proceedings of the IEEE*, vol. 106, no. 3, pp. 343–361, 2018.
- [3] L. O. Inumoh, N. M. Horri, J. L. Forshaw, and A. Pechev, "Bounded gain-scheduled lqr satellite control using a tilted wheel," *IEEE Transactions on Aerospace and Electronic Systems*, vol. 50, no. 3, pp. 1726–1738, 2014.
- [4] X. Wang, G. Wu, L. Xing, and W. Pedrycz, "Agile earth observation satellite scheduling over 20 years: Formulations, methods, and future directions," *IEEE Systems Journal*, vol. 15, no. 3, pp. 3881–3892, 2021.
- [5] W. Lu, W. Gao, B. Liu, W. Niu, D. Wang, Y. Li, X. Peng, and Z. Yang, "Reinforcement learning driven time-sensitive moving target tracking of intelligent agile satellite," *IEEE Transactions on Aerospace and Electronic Systems*, vol. 60, no. 6, pp. 9085–9101, 2024.
- [6] L. Zhao, Z. Lu, K. V. Ling, Y. Hu, K. Zheng, and W. Liao, "Multi-rate cascade spacecraft attitude-orbit integrated state estimation and control framework based on mhe and pwa-mpc," *IEEE Transactions on Aerospace and Electronic Systems*, pp. 1–19, 2025.
- [7] R. J. Caverly, S. D. Cairano, and A. Weiss, "Electric satellite station keeping, attitude control, and momentum management by mpc," *IEEE Transactions on Control Systems Technology*, vol. 29, no. 4, pp. 1475–1489, 2021.
- [8] M. AlandiHallaj and N. Assadian, "Multiple-horizon multiple-model predictive control of electromagnetic tethered satellite system," *Acta Astronautica*, vol. 157, pp. 250–262, 2019.
- [9] Y. Zhou, Y. Hu, K.V. Ling, and F. Ding, "Hybrid two-stage identification-based nonlinear mpc strategy for satellite attitude control," *IEEE Transactions on Aerospace and Electronic Systems*, pp. 1–12, 2025.
- [10] Y. Song, A. Romero, M. Muller, V. Koltun, and D. Scaramuzza, "Reaching the limit in autonomous racing: Optimal control versus reinforcement learning," *Science Robotics*, vol. 8, no. 82, p. eadg1462, 2023.
- [11] M. Kamel, M. Burri, and R. Siegwart, "Linear vs nonlinear mpc for trajectory tracking applied to rotary wing micro aerial vehicles," *IFAC-PapersOnLine*, vol. 50, no. 1, pp. 3463–3469, 2017, 20th IFAC World Congress.
- [12] D. Xu and M. Lazar, "Fast model predictive control of power amplifiers for nanometer precision motion systems," *2023 European Control Conference (ECC)*, Bucharest, Romania, 2023, pp. 1-7.
- [13] P. Krupa, J. Camara, I. Alvarado, D. Limon and T. Alamo, "Real-time implementation of MPC for tracking in embedded systems: Application to a two-wheeled inverted pendulum," *2021 European Control Conference (ECC)*, Delft, Netherlands, 2021, pp. 669-674.
- [14] B. Stevens, F. Lewis, and E. Johnson, *Aircraft Control and Simulation*. Wiley, 2016.
- [15] M. S. C. Tissera, K. J. E. Foo, K.S. Low, S. T. Goh, and R. D. Tan, "Roekf-mpc estimator for satellite attitude and gyroscope bias estimation," *IEEE Transactions on Aerospace and Electronic Systems*, vol. 59, no. 5, pp. 4870–4882, 2023.
- [16] H. J. Ferreau, C. Kirches, A. Potschka, H. G. Bock, and M. Diehl, "qpocases: A parametric active-set algorithm for quadratic programming," *Mathematical Programming Computation*, vol. 6, pp. 327–363, 2014.
- [17] M. S. C. Tissera, K. S. Low, and S. T. Goh, "On-orbit gyroscope bias compensation to improve satellite attitude control performance," in *2021 IEEE Aerospace Conference (50100)*, 2021, pp. 1–10.
- [18] R. Verschuere, G. Frison, D. Kouzoupis, N. van Duijkeren, A. Zanelli, R. Quirynen, and M. Diehl, "Towards a modular software package for embedded optimization," *IFAC-PapersOnLine*, vol. 51, no. 20, pp. 374–380, 2018, 6th IFAC Conference on Nonlinear Model Predictive Control NMPC 2018.
- [19] K. J. E. Foo, M. S. C. Tissera, K. S. Low, and A. Srivastava, "Flitesim: A comprehensive verification and validation environment for small satellite attitude determination and control systems," *IEEE Access*, vol. 13, pp. 109 069–109 086, 2025.
- [20] M. S. C. Tissera, J. W. Chia, K. S. Low, and Y. T. Xing, "A novel simulator for measuring the performance of nanosatellite's attitude control system," in *2016 IEEE Aerospace Conference*, 2016, pp. 1–7.
- [21] K. Foo, M. Tissera, R. Tan, and K. Low, "Agile development of small satellite's attitude determination and control system," in *2023 IEEE Aerospace Conference*, 2023, pp. 1–11.